Available online at www.sciencedirect.com
SCIENCE DIRECT®
Pergamon
Acta Materialia 51 (2003) 4347–4356
Acta MATERIALIA
www.actamat-journals.com

Designing damage-resistant brittle-coating structures: I. Bilayers

Pedro Miranda [a], Antonia Pajares [b], Fernando Guiberteau [a], Yan Deng [c], Brian R. Lawn [d,*]

[a] *Departamento de Electrónica e Ingeniería Electromecánica, Escuela de Ingenierías Industriales, Universidad de Extremadura, 06071 Badajoz, Spain*
[b] *Departamento de Física, Facultad de Ciencias, Universidad de Extremadura, 06071 Badajoz, Spain*
[c] *Department of Materials and Nuclear Engineering, University of Maryland, College Park, MD 20742-2115, USA*
[d] *Materials Science and Engineering Laboratory, National Institute of Standards and Technology, Gaithersburg, MD 20899, USA*

Received 16 January 2003; received in revised form 21 May 2003; accepted 21 May 2003

Abstract

A FEA study of coating/substrate bilayers is conducted as a foundation for damage analysis. Attention is focused on the stresses along the contact axis immediately adjacent to the bilayer interface, where radial cracking or yield in the coating, or yield in the substrate, tend to occur. The stress analysis is used to determine critical loads to initiate each damage mode in terms of basic material properties and coating thickness. Controlling material parameters are strength (brittle mode) and yield stress or hardness (plastic mode). The critical loads are shown to have a simple quadratic dependency on coating thickness, but more complex dependencies on elastic modulus mismatch ratio. Simplified explicit modulus functions afford a route to prediction of the critical loads for design purposes. Implications concerning the design of bilayers for specific applications are discussed.
Published by Elsevier Ltd on behalf of Acta Materialia Inc.

Keywords: Bilayers; Brittle-coatings; Cracking; Critical loads; Finite element analysis; Plasticity

1. Introduction

Laminate structures with functional stiff and hard outer layers (typically ceramics) on compliant or soft support bases (polymers, metals, or even soft ceramics) are representative of many engineering coating systems (cutting tools, thermal barrier coatings, ceramic armor, laminated windows, eye glasses, electronic packaging devices, hard disks) and biomechanical systems (shells, teeth, dental crowns) [1]. The simplest form of such structures is a bilayer—a coating on a substrate. In some functional systems (e.g. dental crowns) the structure is a trilayer (or even multilayer), with an intermediate support core layer. The outer layers shield the underlying substrate from external loads, but any one layer may be susceptible to damage above some critical applied load. Because adjacent layers may consist of different material types—ceramic, metal, polymer or composite—the damage modes

* Corresponding author.
E-mail address: brian.lawn@nist.gov (B.R. Lawn).

1359-6454/03/$30.00 Published by Elsevier Ltd on behalf of Acta Materialia Inc.
doi:10.1016/S1359-6454(03)00290-8

can be varied and complex. An understanding of these modes is critical to the design of longer-lifetime systems.

Several damage modes have been identified in bilayers in concentrated loading. Near-contact modes, e.g. cone (or outer ring) cracking or quasi-plasticity, can occur in the top surfaces, as in monoliths [2–5]. However, such top-surface modes are dominant only in thicker coatings [2], and can in any case be avoided by ensuring sufficiently blunt or soft contacts, so we shall regard them as secondary. More insidious in thinner, brittle coatings are subsurface radial cracks [1–3,5,6]. Radial cracks initiate at the coating/substrate interface, and are associated with coating flexure beneath the contact. They can extend long lateral distances with increasing load. In softer coatings, fracture at the undersurface may be supplanted by local yield. Yet another important mode is yield in the substrate itself, particularly in soft metals. In cases where the substrate is stiffer than the coating (e.g. porcelain/metal crowns), substrate yield can act as an essential precursor to radial cracking in the overlying coating [7]. Such plasticity may also cause delamination of the coating/substrate interface. Whereas the activation of any one damage mode may not lead to immediate failure of the bilayer, it signals the beginning of the end of the useful lifetime of the structure (especially biomechanical structures)—the issue is then one of damage prevention rather than damage containment [1,3].

Accordingly, a primary goal in the analysis of bilayers is the development of explicit relations for the critical loads to activate subsurface coating cracking or yield, and substrate yield, in terms of key geometrical and material variables. Existing relations suggest a common quadratic dependency of the critical loads on coating thickness (typical of point-contact and flexure fields), and somewhat slower dependencies on modulus ratio [1]. However, these dependencies, especially those associated with modulus mismatch, remain to be fully validated. The same relations also predict a linear dependence on fracture strength [4] or yield stress [7] of the coating and substrate materials, depending on the damage mode.

The present study is divided into two parts. Part I deals with bilayers, Part II with trilayers. Finite element analysis (FEA) is used to evaluate the important stress components in the layers, and thence to determine critical load relations for the different damage modes by equating maximum tensile and shear stress components to material strength (fracture) or yield stress (plasticity). The bilayer solutions are used to validate the quadratic coating thickness dependency in the existing critical load relations, and to examine further the modulus dependency. Apart from their intrinsic importance, bilayer solutions provide an essential starting point for analysis of trilayers. As we shall indicate in Part II, trilayers are subject to similar damage modes, in either outer or inner layers depending on thickness and modulus ratios [1]. Finally, consideration will be given as to how the results may be used as a basis for materials design of layer structures.

2. Stress analysis

2.1. Damage modes

Consistent with a damage prevention philosophy [1,3], we focus on first-damage conditions in the bilayer system of Fig. 1. A coating layer of thick-

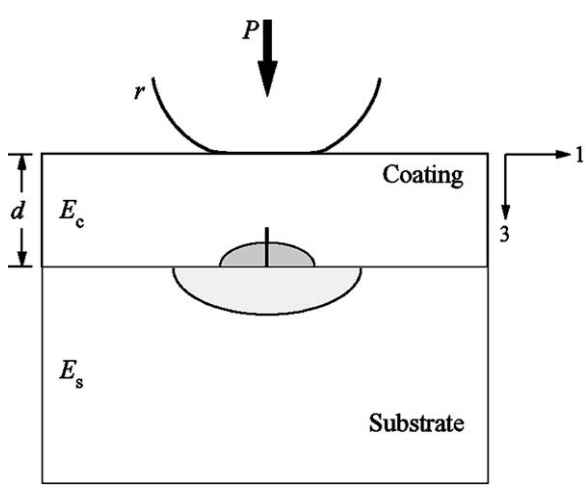

Fig. 1. Schematic of damage in bilayers of coating thickness d and modulus E_c and substrate of modulus E_s, from contact at top surface with sphere of radius r at load P. Principal subsurface damage modes are radial cracking and yield (shaded) in coating and substrate immediately adjacent to interface.

ness d and modulus E_c is bonded to a thick substrate ($\gg d$) of modulus E_s. The bilayer is in contact with a sphere of radius r at load P at the top surface. It is assumed that the contact radius remains small compared to d, so that the loading is effectively point-force in nature. Principal subsurface damage modes immediately adjacent to the interlayer interface and along the contact axis are as follows [6,7]: in the coating, radial fracture or plasticity (or quasiplasticity in ceramic); in the substrate, plasticity (or quasiplasticity). Illustrative section views from previous studies are shown in Fig. 2 (all at loads well above threshold in order to demonstrate the various damage modes): (a) a fine-grain micaceous glass–ceramic (F-MGC) bonded to a filled-polymer composite substrate (simulating tooth enamel/dentin) [8], showing subsurface radial cracks and outer surface ring cracks in the coating; (b) porcelain fused to Pd-alloy metal (simulating metal-core dental crowns), showing yield in the substrate and cone and radial fracture in the coating [9]; (c) porcelain fused to alumina (representing dental all-ceramic crowns), showing only surface cone cracks in the coating [8].

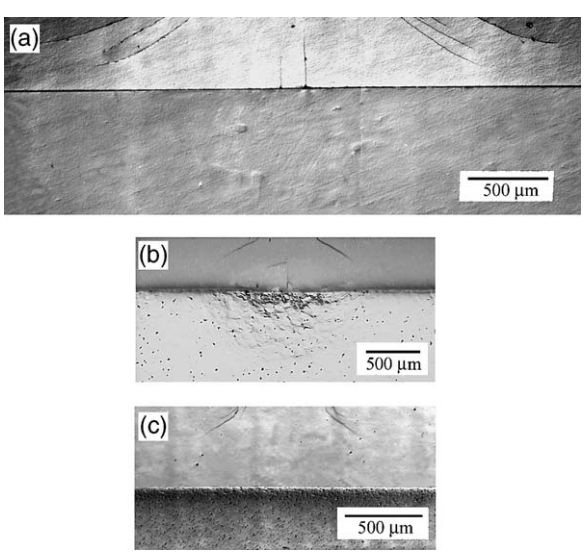

Fig. 2. Section views of damage in flat ceramic-coating/substrate bilayers: (a) F-MGC/filled-polymer, WC sphere indenter $r = 3.18$ mm at $P = 250$ N [8]; (b) porcelain/Pd-alloy, $r = 2.38$ mm at $P = 500$ N [9]; (c) porcelain/glass-infiltrated-alumina, $r = 3.18$ mm at $P = 500$ N [8]. Bonded-interface specimens.

Evaluation of the damage modes begins in this section with detailed FEA of relevant normal and von Mises stresses. Equating maximum values of these stresses to the material strength (cracking) or yield stress (plasticity) then enables determination of pertinent critical load relations (Section 3).

2.2. Finite element analysis

A FEA scheme described in a previous study [10] is used to determine stress states in the contact configuration of Fig. 1. The system considered is a WC indenter of radius r in frictionless axisymmetric contact with the top surface of a coating of specified thickness d, modulus E_c and Poisson's ratio ν_c, bonded to a thick substrate of specified modulus E_s and Poisson's ratio ν_s. The net external dimensions of the bilayer structures are 16 mm radius and 14 mm thickness, with minimum element dimension 4 μm in the vicinity of the interfaces. The sphere is loaded incrementally to peak value, and the stresses are evaluated along the contact axis at chosen intervals. Representative Poisson's ratios $\nu_c = 0.22$ and $\nu_s = 0.30$ are used in the basic calculations. It is assumed in the calculations that the stresses are elastic everywhere up to the onset of yield or fracture.

Values of the principal stresses σ_1 ($=\sigma_2$) and σ_3 along the contact axis and corresponding von Mises stresses $\sigma_{13} = \{\frac{1}{2}[(\sigma_1-\sigma_2)^2 + (\sigma_2-\sigma_3)^2 + (\sigma_1-\sigma_3)^2]\}^{1/2} = \sigma_1-\sigma_3$ are shown in Fig. 3 for $E_c = 70$ GPa (e.g. glass or porcelain coatings—Table 1) and (a) $E_s = 7$ GPa or (b) $E_s = 700$ GPa, for fixed $d = 2$ mm, $r = 3.18$ mm and $P = 25$ N. Note the pronounced nonlinearity in the stress distributions across the section, indicating significant departures from a simple flexural stress state [11]. Note also that whereas σ_3 is continuous across the interface, σ_1 and σ_{13} have distinct discontinuities, highlighting the influence of elastic mismatch. For the modulus ratio $E_c/E_s = 10$ (Fig. 3a), the near-interface σ_1 stress in the coating is tensile and dominates that in the substrate (shielding); for $E_c/E_s = 0.1$ (Fig. 3b), the same near-interface σ_1 stress is compressive in both the coating and substrate [8].

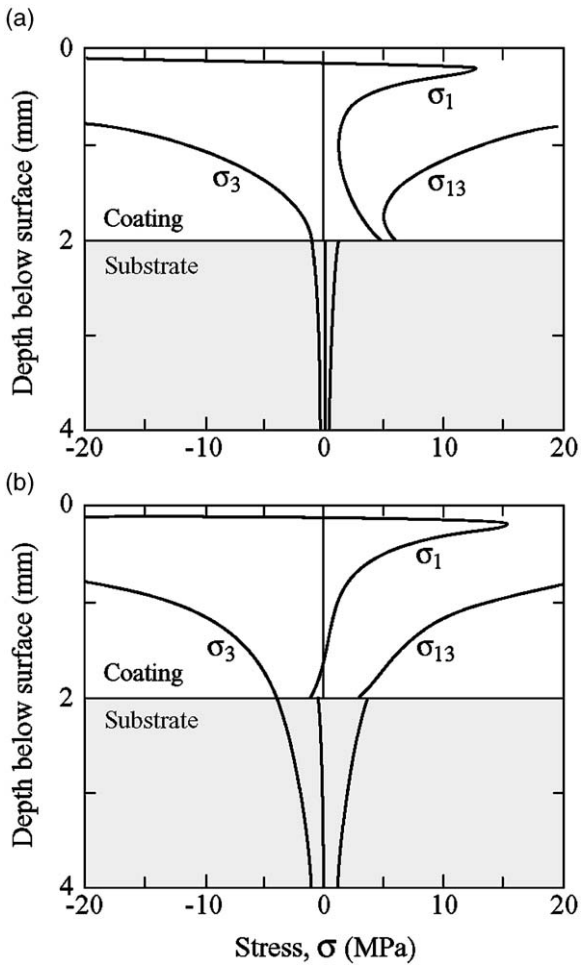

Fig. 3. FEA-generated stresses σ_1, σ_3, and σ_{13} along contact axis, for E_c = 70 GPa and (a) E_s = 7 GPa or (b) E_s = 700 GPa (ν_c = 0.22, ν_s = 0.30), at d = 2 mm, r = 3.18 mm and P = 25 N. Note nonlinear stress distributions across section.

2.3. Stress relations

Principal normal stresses σ_1^c and von Mises stresses σ_{13}^c at the coating lower surface and σ_{13}^s at the substrate upper surface are plotted in Fig. 4 as a function of d^{-2}, for E_c = 70 GPa and E_s = 2.23 GPa (glass/polycarbonate, Table 1) and r = 3.18 mm at P = 25 N. Data points are FEA calculations and the solid lines are linear best fits. Analogous plots in Fig. 5 of σ_1^c versus P/d^2 for selected r/d at fixed interface depth d = 2 mm indicate nonlinearities at large P, especially at large r/d. Similar trends are observed in the other stress components. In the interest of simplicity, our ensuing stress evaluations will be confined to the linear regions of small P and r/d. Within these linear regions, the plots in Figs. 4 and 5 confirm $\sigma(d)$ relations of general form

$$\sigma = (P/d^2)\Sigma(E_c/E_s) \tag{1}$$

with $\Sigma(E_c/E_s)$ separable modulus-dependent functions.

This leaves the functions $\Sigma(E_c/E_s)$ to be determined. Fig. 6 plots the quantity $\Sigma = \sigma d^2/P$ for each pertinent stress component as a function of modulus ratio E_c/E_s, for the same system represented in Fig. 4 but for variable E_s. Data points are FEA calculations. Note that the E_c/E_s axis in Fig. 6 is logarithmic, so the modulus dependence is relatively slow. In the region $E_c/E_s > 1$ the tensile stress σ_1^c and von Mises stress σ_{13}^c dominate, so damage at the coating undersurface is favored; at $E_c/E_s < 1$ the von Mises stresses σ_{13}^c and σ_{13}^s dominate, so some form of yield is favored. The damage mode that dominates at any given value of E_c/E_s will depend on the relative values of coating tensile strength and coating/substrate yield stresses (Section 3).

The stresses σ_1^c and σ_{13}^s warrant particular consideration, because of the attention paid in earlier bilayer studies to ceramic coating cracking [1,6] and metal substrate yield [7,9]. The stress σ_{13}^c pertaining to coating yield is also of interest, if only because of its later relevance to trilayers (Part II). In these cases the FEA data can be approximated by simple functions, represented as the solid lines in Fig. 6. Note that σ_1^c undergoes a transition from compression to tension at $E_c/E_s \approx 0.7$. In the tension region, the data for this stress may reasonably be fitted by a straight line, in accordance with the relation for plates on elastic foundations [11,12]

$$\sigma_1^c d^2/P = \Sigma_1^c = (1/B)\log(CE_c/E_s) \quad (1 < E_c/E_s < 100) \tag{2a}$$

with values B = 1.35 and C = 1.00. Data for the σ_{13}^c stress may similarly be fitted by two straight lines

Table 1
Properties of representative materials[a]

Material	Modulus E (GPa)	Hardness H (GPa)	Strength S (MPa)
Ceramic			
Glass (abraded)	73	5.2	110
Porcelain (dental)	68	6.2	110
Zirconia (Y-TZP)	205	12.0	1450
Mica glass–ceramic (F-MGC)	70.5	3.8	325
Mica glass–ceramic (C-MGC)	51.5	2.7	125
Alumina (glassy phase)	270	12.3	550
Metal			
Pd-alloy (dental)	126	2.0	
Co-alloy (dental)	231	3.0	
Tungsten carbide (indenter)	614	19	
Polymer			
Polycarbonate	2.3	0.3	
Glass-filled polymer (dental)	10	0.8	
Tooth dentin	16	0.6	

[a] Data from Ref. [1].

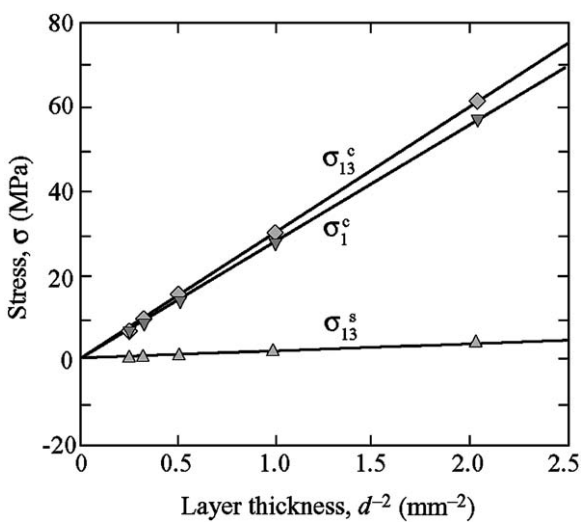

Fig. 4. FEA-generated stresses σ_1 and σ_{13} at coating/substrate interface as function of d^{-2} for $E_c = 70$ GPa and $E_s = 2.23$ GPa ($\nu_c = 0.22$, $\nu_s = 0.30$), $r = 3.18$ mm at $P = 25$ N. Note linear responses over data range.

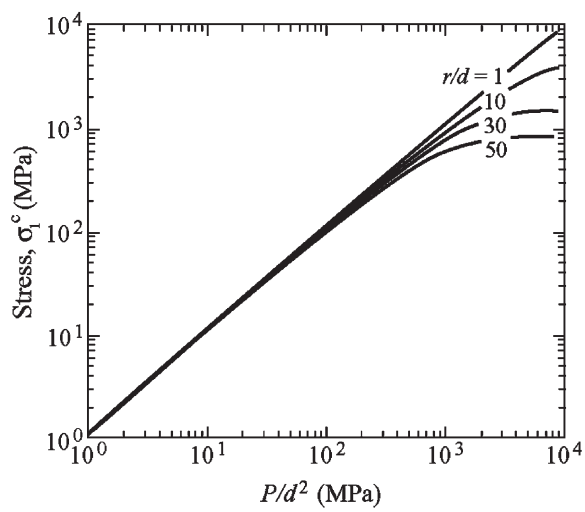

Fig. 5. FEA-generated stress σ_1^c at coating/substrate interface as function of P/d^2 at $d = 2$ mm, for $E_c = 70$ GPa and $E_s = 2.23$ GPa ($\nu_c = 0.22$,$\nu_s = 0.30$), at specified r/d values. Note nonlinear responses at higher P and r/d.

$$\sigma_{13}^c d^2/P = \Sigma_{13}^c = (1/D)\log(KE_c/E_s)$$
$$(1 < E_c/E_s < 1000) \qquad (2b)$$
$$= (1/D)\log(K) \quad (E_c/E_s < 1)$$

with $D = 2.08$ and $K = 11.0$. The σ_{13}^s stress data may be approximated over the entire range of E_c/E_s by the sigmoidal function [7]

$$\sigma_{13}^s d^2/P = \Sigma_{13}^c = 1/G(1 + ME_c/E_s), \qquad (2c)$$

with $G = 1.74$ and $M = 0.178$. To these expressions

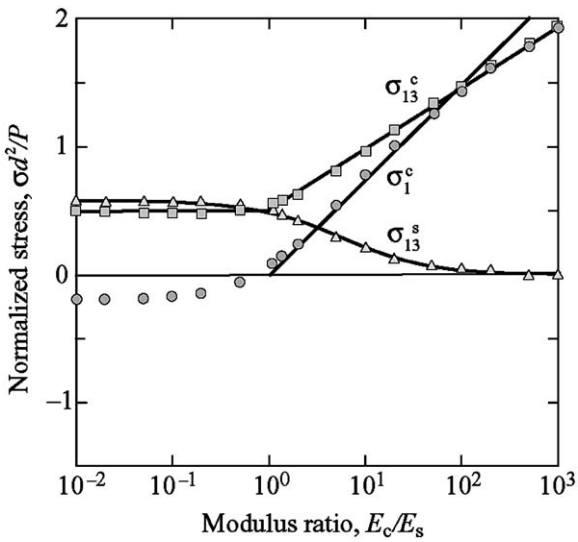

Fig. 6. Stress quantities $\sigma d^2/P$ at coating/substrate interface as function of E_c/E_s, for fixed E_c = 70 GPa and variable E_s (ν_c = 0.22, ν_s = 0.30), at r = 3.18 mm and P = 25 N. Data points are FEA calculations, solid lines are best fits of Eq. (2a–c).

may be added a sigmoidal fit to raw σ_3^c data (not shown in Fig. 6), for use in Part II:

$$\sigma_3^c d^2/P = \Sigma_3^c = 1/g[1 + m(E_c/E_s)^p] \quad (2d)$$

with $g = -1.43$, $m = 0.46$ and $p = 0.79$.

3. Critical loads for damage modes

Now impose critical stress criteria to determine threshold load relations for each damage mode in Fig. 1 in terms of practical material properties. Let any given damage mode initiate at a stress $\sigma = \sigma_{crit}$ corresponding to a critical load $P = P_{crit}$ in Eq. (1). Then

$$P_{crit} = \sigma_{crit} d^2/\Sigma(E_c/E_s) \quad (3)$$

where σ_{crit} is identifiable with strength S (tensile stress) or yield stress Y (von Mises stress) in the coating and substrate, so that

$$P_{crit} = P_R^c, \quad \sigma_{crit} = S_c, \quad \Sigma = \Sigma_1^c \quad (4a)$$

$$P_{crit} = P_Y^c, \quad \sigma_{crit} = Y_c, \quad \Sigma = \Sigma_{13}^c \quad (4b)$$

$$P_{crit} = P_Y^s, \quad \sigma_{crit} = Y_s, \quad \Sigma = \Sigma_{13}^s \quad (4c)$$

with the Σ functions given approximately in Eq. (2a–c). Eqs. (3) and (4a–c) may be used to determine which interface damage mode occurs first in any given bilayer system. Illustrative case studies will be considered in the Discussion.

The well-documented indentation hardness relation $H = cY$ ($c \approx 3$) [13] can be a useful adjunct in evaluating the yield stresses in Eq. (4b,c), especially for ceramics where yield stress measurements are otherwise difficult [4].

4. Discussion

We have conducted a stress analysis using FEA as a basis for determining the critical conditions to activate damage modes in bilayer structures. Particular attention has been paid to damage modes in the immediate vicinity of the coating/substrate interface. Secondary damage modes that can occur in the near-contact region at the top surface [3–5] have not been considered thus far in this study, since they become important only in the limits of thick coatings and sharp contacts. The near-interface modes include radial cracking and yield at the lower surface of the coating, and yield in the upper surface of the substrate. These latter modes are assumed to activate when the principal tensile or von Mises stresses equal the bulk strength S or yield stress Y (=H/3) of the pertinent material. This approach enables us to establish relatively simple relations for the near-interface damage thresholds. Thus the critical loads for all the near-interface modes in Eq. (3) have an universal quadratic dependence on coating thickness d (Fig. 4), at least within the linear region (Fig. 5), typical of Boussinesq point-contact and plate flexure stress fields [1]. They also have a linear dependence on S or Y. As we shall demonstrate in Part II, these simple and explicit dependencies on layer thicknesses and key material parameters are preserved in trilayers.

The modulus dependence is more complex (Fig. 6), and is represented in Eq. (2a–d) by simple semi-empirical functions. In conjunction with Eqs. (3) and (4a–c), these functions give expressions for the critical loads to produce radial cracking and yield in coatings, and yield in substrates:

$$P_R^c = BS_c d^2/\log(CE_c/E_s) \quad (1 < E_c/E_s < 100) \tag{5a}$$

$$P_Y^c = \frac{1}{3}DH_c d^2/\log(KE_c/E_s) \quad (1 < E_c/E_s < 1000)$$

$$= \frac{1}{3}DH_c d^2/\log(K) \quad (E_c/E_s < 1) \tag{5b}$$

$$P_Y^s = \frac{1}{3}GH_s d^2(1 + ME_c/E_s) \tag{5c}$$

Eq. (5a) has previously been used to quantify radial cracking in ceramic coatings bonded to compliant substrates [1,6], and Eq. (5c) likewise to quantify yield in metal substrates overlaid with hard coatings [7,9].

It should be emphasized that while radial fracture is arguably the most deleterious mode in bilayers in concentrated loading the yield modes, when they do occur, are hardly benign. Yield can enhance plate flexure with subsequent radial cracking in ceramic coatings, or cause interface delamination at higher loads [7]. In such cases a nonlinear stress analysis with input of elastic–plastic constitutive relations is needed to evaluate the critical conditions [1]. Thus, while the onset of first damage (fracture or yield) may not lead to imminent failure, it signals ultimate failure. As such, the critical loads P_Y and P_R are both useful quantities in bilayer design. The question as to whether coating radial fracture occurs before coating or substrate plasticity may be addressed by combining Eqs. (3) and (4a–c) to give

$$P_Y^c/P_R^c = (Y_c/S_c)(\Sigma_1^c/\Sigma_{13}^c) \tag{6a}$$

$$P_Y^s/P_R^c = (Y_s/S_c)(\Sigma_1^c/\Sigma_{13}^s) \tag{6b}$$

for any fixed coating thickness d. The quantities P_Y^c/P_R^c and P_Y^s/P_R^c may then be taken as indices of brittleness for any specified value of E_c/E_s: if both indices >1, the response is brittle; if either index <1, the response is plastic. Similarly, the issue of whether plasticity is more likely to occur first in the coating or substrate may be decided by dividing Eq. (6b) into (6a):

$$P_Y^c/P_Y^s = (Y_c/Y_s)(\Sigma_{13}^s/\Sigma_{13}^c) \tag{6c}$$

If $P_Y^c/P_Y^s > 1$, plasticity occurs first in the substrate; if <1, it occurs first in the coating. In this context, the ratios Y_c/S_c, Y_s/S_c and Y_c/Y_s are useful damage mode indicators.

Eq. (6a–c) provides a basis for mapping the susceptibilities of bilayer structures to competing subsurface damage modes. Of primary interest is how the relative critical loads depend on the modulus ratio E_c/E_s. For the question as to whether coating radial fracture occurs before coating or substrate plasticity, impose the conditions $P_Y^c = P_R^c$ and $P_Y^s = P_R^c$ in Eqs. (6a) and (6b), corresponding to $Y_c/S_c = \Sigma_{13}^c(E_c/E_s)/\Sigma_1^c(E_c/E_s)$ and $Y_s/S_c = \Sigma_{13}^s(E_c/E_s)/\Sigma_1^c(E_c/E_s)$. Loci of these equalities plotted as the solid lines in Fig. 7a and b, evaluated using Eq. (5a–c), distinguish domains in which each mode dominates. Also plotted as data points are values of Y_c/S_c and Y_s/S_c for selected coating/substrate bilayer systems, using data from Table 1 along with $H = 3Y$. (In these figures, bilayers with metal coatings are not plotted because of the unavailability of meaningful tensile strength values S_c, but will tend to lie in the yield domains at the bottom of the plots.) Coating radial fracture is excluded for relatively stiff substrates, $E_c/E_s<1$ in Fig. 7a and b (recall transition from tension to compression of σ_1^c in Fig. 6). For compliant substrates, radial fracture can only occur first if Y_s/S_c and Y_c/S_c are sufficiently large that the appropriate data point lies within the upper-right domains in Fig. 7a and b, where flexural stresses become dominant. Note that radial fracture is altogether excluded as a first damage mode in the domain $Y_c/S_c<1$, independent of E_c/E_s (see Fig. 7b). For systems located in the yield regions of Fig. 7a and b, the issue as to whether yield is more likely to occur first in the coating or substrate is addressed by the analogous plot of $Y_s/Y_c = \Sigma_{13}^s/\Sigma_{13}^c$ in Fig. 7c. For stiff substrates ($E_c/E_s<1$) yield will typically occur first in the softer material. For more compliant substrates ($E_c/E_s>1$), yield is more strongly favored in the coating, again where flexural stresses become increasingly dominant.

In this context, the quantities Y_c/S_c and Y_s/S_c (or H_c/S_c and H_s/S_c) may be regarded as useful indices of brittleness for a given bilayer system, for any specified value of E_c/E_s. These indices are analogous to the quantities H/T (T = toughness, K_{IC})

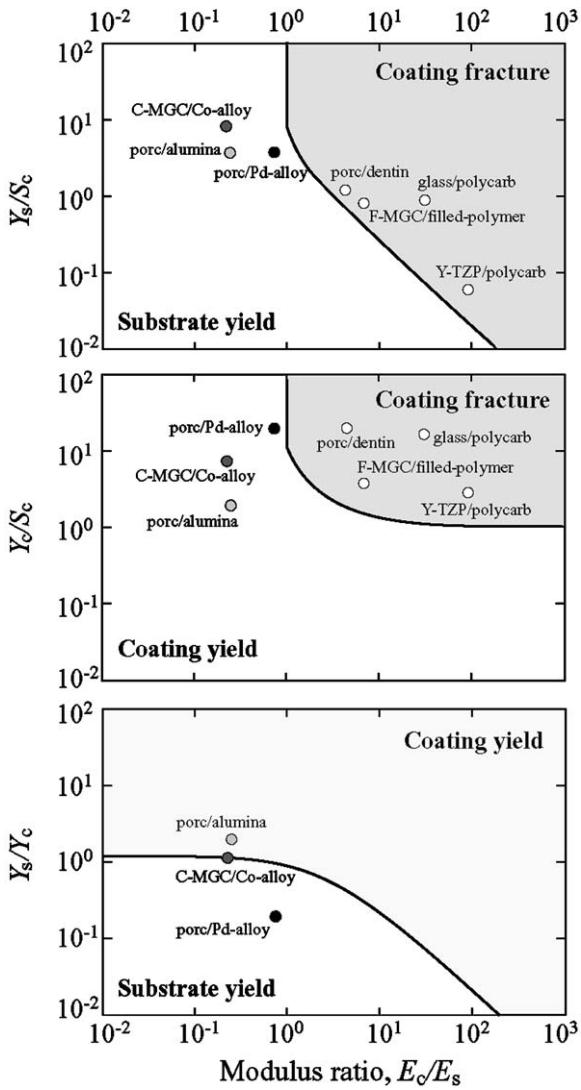

Fig. 7. Plots of (a) Y_s/S_c, (b) Y_c/S_c and (c) Y_s/Y_c versus E_c/E_s for representative material systems (Table 1). Solid lines delineate domains of first radial cracking or yield.

used to define brittleness in indentation fracture configurations in monolithic materials [4,14,15]—replacement of toughness T with strength S here simply reflects a transition in stress state from that of monolith elastic–plastic contact (where strong stress gradients promote a more stabilized crack evolution [3,5,6]) to one of plate flexure (where crack initiation is abrupt).

It is of interest to establish the coating thickness domains in which the above near-interface damage modes dominate top-surface modes using conventional design diagrams [1,5,6]. The lowest of the critical loads P_R^c, P_Y^c or P_Y^s for near-interface damage may first be determined from Fig. 7 for each bilayer system. This critical load may then be determined, along with the critical load for near-contact cone cracking (or plasticity or quasiplasticity), as a function of coating thickness d. Recall that all coating/substrate interface modes have a common quadratic d dependence in Eq. (3), so the functions $P_R^c(d)$, $P_Y^c(d)$ or $P_Y^s(d)$ will plot as parallel inclined lines of slope 2 in logarithmic coordinates. The top-surface modes, on the other hand, are relatively independent of d [6], and so constitute an upper bound. Accordingly, first-damage functions are plotted in Fig. 8 (solid lines) for the F-MGC/filled-polymer, porcelain/Pd-alloy and porcelain/alumina bilayers illustrated in Fig. 2 using parameters from Table 1 in Eq. (5a–c), along with previous data for cone cracks [5] (horizontal dashed line, representative of both F-MGC and

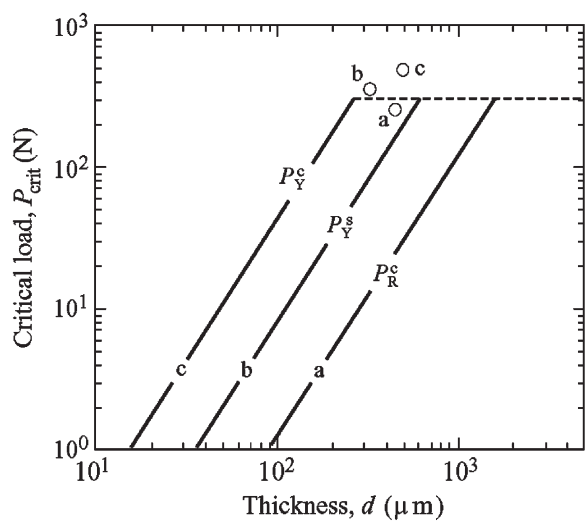

Fig. 8. Design diagram, showing plots of critical loads P_Y^c, P_R^c and P_Y^s computed from Eq. (5a–c) as function of coating thickness d (solid lines), for (a) F-MGC/filled-polymer, (b) porcelain/Pd-alloy, and (c) porcelain/alumina bilayers. Horizontal line is upper bound at high d, where top-surface damage occurs first (from Ref. [5]). Note that each system initiates a different subsurface damage mode in the low d region. Points represent loads and thicknesses corresponding to the micrographs in Fig. 2.

porcelain). (The data points included in Fig. 8 simply indicate the operative loads for the coating thicknesses in the micrographs of Fig. 2.) It is evident that subsurface damage modes are highly deleterious in thinner coating systems. Note that the predicted first-damage subsurface mode is different for each material combination—radial cracking, substrate yield and coating yield (cf. Fig. 7). This result highlights the importance of the support layer not only in influencing the critical loads for damage but also in controlling the modes themselves.

While providing a useful indicator of the overload conditions pertinent to Fig. 2, data points of the kind included in Fig. 8 strictly should not be taken as a predictor of other than first-damage, because the onset of any damage mode may alter stress distributions and thus influence conditions for initiation of subsequent modes. In the case of Pd-alloy substrates in Fig. 2b, for instance, radial cracks are evident even though the elasticity analysis indicates compression at the coating undersurface ($P_R^c \rightarrow \infty$)—tensile stresses are generated in this instance only because of precursor substrate yield. The issue of damage evolution beyond first fracture or yield requires a more complex analysis than given here.

We reiterate that the FEA data generated in Fig. 6 and thereby in Fig. 7 were obtained for nominal values of Poisson's ratios ($\nu_c = 0.22$, $\nu_s = 0.30$). Variations in these input parameters can lead to data shifts in Fig. 6. Accordingly, although most practical ceramic/substrate bilayer systems have Poisson ratios close to those used here, care should be taken when using our fitted coefficients in systems where Poisson's ratios differ significantly.

In principle, it should be possible to invert Eq. (5a–c) to determine material strengths or yield stresses from experimental critical load data. This could be valuable for thin coating structures where it is difficult to obtain free-standing specimens. However, while the onset of radial fracture is relatively easy to detect as a well-defined "pop-in" event, either visually or from load-drop traces or acoustic emissions, the onset of yield tends to be more continuous and consequently harder to detect. We may also expect some differences in properties measured this way from those measured on traditional bulk specimens, raising questions as to the validity of simple critical stress criteria for fracture and yield. Sources of difference include: assumption of specific values of Poisson's ratio in the FEA computations (previous paragraph); assumption of point-contact loading (e.g. Fig. 5) [11]; stress gradients across the flaw [16] and effect of statistics in flaw distributions (both increasingly important at smaller d) [17]; existence of rate effects in radial cracking [18]; enhanced coating flexure from any compliant adhesive used in the interlayer bonding [19], or superposed residual stresses in the coating associated with chemical contraction or expansion in the same adhesive [20,21]; adhesive filling of coating undersurface flaws at the epoxy-bonded interface [12]. On the other hand, "effective" strengths and yield stresses evaluated from bilayer critical load data will be more relevant to practical coating configurations in concentrated loading than will their bulk-value counterparts.

The bilayer analysis presented in this study constitutes an essential starting point for the analysis of trilayers, to be considered in Part II.

Acknowledgements

This study was supported by internal funds from NIST, and by grants from the US National Institute of Dental and Craniofacial Research (Grant PO1 DE10976), the Junta de Extremadura-Consejeria de Educacion Ciencia y Tecnologia y el Fondo Social Europeo, Spain (Grant IPR00A084) and Secretaria de Estado de Educacion y Universidades, Spain.

References

[1] Lawn BR, Deng Y, Miranda P, Pajares A, Chai H, Kim DK. J Mater Res 2002;17:3019.
[2] Chai H, Lawn BR, Wuttiphan S. J Mater Res 1999;14:3805.
[3] Lawn BR, Lee KS, Chai H, Pajares A, Kim DK, Wuttiphan S et al. Adv Eng Mater 2000;2:745.
[4] Rhee Y-W, Kim H-W, Deng Y, Lawn BR. J Am Ceram Soc 2001;84:561.
[5] Deng Y, Lawn BR, Lloyd IK. J Biomed Mater Res (Appl Biomater) 2002;63:137.

[6] Rhee Y-W, Kim H-W, Deng Y, Lawn BR. J Am Ceram Soc 2001;84:1066.
[7] Zhao H, Hu X, Bush MB, Lawn BR. J Mater Res 2001;16:1471.
[8] Jung YG, Wuttiphan S, Peterson IM, Lawn BR. J Dent Res 1999;78:887.
[9] Zhao H, Hu XZ, Bush MB, Lawn BR. J Mater Res 2000;15:676.
[10] Miranda P, Pajares A, Guiberteau F, Cumbrera FL, Lawn BR. J Mater Res 2001;16:115.
[11] Timoshenko S, Woinowsky-Krieger S. Theory of plates and shells, 2nd ed. New York: McGraw-Hill, 1959.
[12] Kim H-W, Deng Y, Miranda P, Pajares A, Kim DK, Kim H-E, Lawn BR. J Am Ceram Soc 2001;84:2377.
[13] Tabor D. Hardness of metals. Oxford: Clarendon Press, 1951.
[14] Lawn BR, Marshall DB. J Am Ceram Soc 1979;62:347.
[15] Puttick KE. J Phys D: Appl Phys 1979;12:L19.
[16] Chai H. Int J Solids Struct 2003;40:591.
[17] Miranda P, Pajares A, Guiberteau F, Cumbrera FL, Lawn BR. Acta Mater 2001;49:3719.
[18] Lee C-S, Kim DK, Sanchez J, Miranda P, Pajares A, Lawn BR. J Am Ceram Soc 2002;85:2019.
[19] Chai H, Lawn BR. J Mater Res 2000;15:1017.
[20] Leevailoj C, Platt JA, Cochran MA, Moore BK. J Prosthet Dent 1998;80:699.
[21] Choi KK, Condon JR, Ferracane JL. J Dent Res 2000;79:812.